Applied Surface Science 301 (2014) 70–78

Contents lists available at ScienceDirect

Applied Surface Science

journal homepage: www.elsevier.com/locate/apsusc

Temperature dependent $LiNbO_3(0\,0\,0\,1)$: Surface reconstruction and surface charge

S. Sanna*, R. Hölscher, W.G. Schmidt

Lehrstuhl für Theoretische Physik, Universität Paderborn, 33098 Paderborn, Germany

ARTICLE INFO

Article history:
Received 31 October 2013
Received in revised form 13 January 2014
Accepted 17 January 2014
Available online 27 January 2014

Keywords:
Ferroelectrics
Density functional theory
DFT
$LiNbO_3$
Surface charge

ABSTRACT

The polar $(0\,0\,0\,1)$ surface of stoichiometric $LiNbO_3$ undergoes a series of structural transformations with temperature. This complex behavior mirrors the action of different charge compensation mechanisms at specific temperatures. In this work the surface charge associated to various surface terminations is estimated from first-principles calculations. All the thermodynamically stable terminations are found to lower the polarization charge, showing that the surface charge compensation is a major driving force for the observed morphologic transformations.

1. Introduction

The polar surfaces of ferroelectric oxides have attracted the attention of scientists and engineers for a long time. Indeed, a variety of applications exploiting the strong electric fields at the surfaces have been realized. Among the mostly employed ferroelectric surfaces, the lithium niobate $LiNbO_3(0\,0\,0\,1)$ plays a prominent role [1]. It is in fact widely exploited, e.g. for the realization of surface acoustic wave devices [2] or to grow group III nitrides with spatially varied polarity control [3]. Novel applications exploit the possibility (exclusive to ferroelectrics) to switch the polarization, and thus the chemistry [4], of the $(0\,0\,0\,1)$ surface. Artificial photosynthesis [5], photocatalytic dye decolorization [6] as well as activation of charged biomolecules [7] on LN surfaces have been demonstrated recently. Furthermore the high surface electric fields were found to efficiently pole electro-optic polymers [8] and to lead to the reversible fragmentation and self-assembling of nematic liquid crystals [9].

Despite many exciting applications, little detailed information on the LN surface atomic structure is available. Yun et al. [10] investigated $(0\,0\,0\,1)$ surfaces at ambient conditions by electron diffraction, and found no indication for reconstructions. Ion scattering spectroscopy suggested that both $(0\,0\,0\,1)$ surfaces are oxygen terminated [10], while coaxial impact-collision ion scattering suggested a Nb surface termination [11,12]. Atomic scale investigations are hindered by the extremely challenging preparation and analysis conditions of strongly polar surfaces of insulating materials, though. While reconstructions at the weakly polar $SrTiO_3(0\,0\,1)$ and $BaTiO_3(0\,0\,1)$ surfaces have been recently demonstrated by scanning tunneling [13,14] and transmission electron [15] microscopy, charging effects prohibit the application of electron tunneling or diffraction techniques and unscreened surface charges hinder atomic force microscopy in LN. Thus, the atomic structure of the $LiNbO_3$ surface remained for a long time experimentally inaccessible. A breakthrough was achieved by Rode et al. [16] performing the AFM measurement in liquid environment, in order to screen the AFM tip from the surface charges. This allowed for the first time true atomic resolution imaging of the $(0\,0\,0\,1)$ surfaces. No surface reconstruction was revealed in stoichiometric samples annealed at 1270 K. Successively, measurements on samples annealed at different temperatures showed a series of structural transformations, including a $\sqrt{7} \times \sqrt{7}$ R19° surface reconstruction [17], stable only in a limited temperature range. The evolution of the surface structure with increasing temperature was interpreted as the result of the interplay between different charge compensation mechanisms. At temperatures below 870 K the polarization charge is compensated by foreign adsorbates. However, if the temperature is sufficiently high to drive off the adsorbates, surface reconstructions are formed to compensate the surface charge. Finally, after annealing above 1270 K any reconstruction disappears. This temperature is rather close to the Curie temperature of LN ($\vartheta_C \approx$ 1480 K [1]), so that the

* Corresponding author. Tel.: +49 05251602333; fax: +49 05251603435.
E-mail address: simone.sanna@uni-paderborn.de (S. Sanna).

0169-4332/$ – see front matter © 2014 Elsevier B.V. All rights reserved.
http://dx.doi.org/10.1016/j.apsusc.2014.01.104

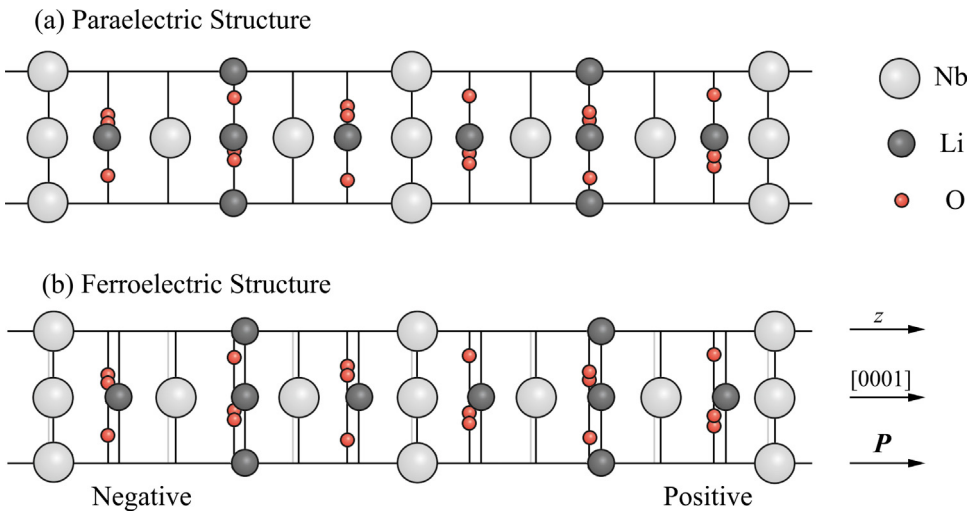

Fig. 1. Schematic representation of the paraelectric (a) and ferroelectric (b) phases of $LiNbO_3$ along the [0 0 0 1] crystallographic direction. In the ferroelectric phase Li and Nb atomic layers are shifted with respect to the oxygen sublattice along the crystal *z*-axis. The gray lines in the ferroelectric phase represent the position of the corresponding atomic layer in the paraelectric phase.

spontaneous polarization, and thus the surface charge, are strongly reduced (pyroelectricity). *Ab initio* thermodynamics based on density functional theory (DFT) calculations pointed out that various reconstructions might be formed at specific conditions [17].

In this work we propose an approximate method to estimate the surface charge within the density functional theory (DFT), and apply it to the thermodynamically stable surface reconstructions, in order to determine the associated surface charge. Thereby we rely on the structural models proposed in Ref. [17]. Our calculations indicate that all the thermodynamically stable surface reconstructions formed at different temperatures reduce the surface charge, suggesting that the compensation of polarization charge is a driving force for the observed structural modifications.

2. Methodology

The determination of the surface polarization charge within the DFT is a delicate task, both due to the vague definition of surface layer and due to the limitations introduced by the supercell approach. This approach is very convenient for the simulation of periodic 3D systems such as bulk structures. However, it suffers from some long-ranging interactions between artificial images in 2D system such as surfaces. A vacuum layer has to be included in the supercell in order to break the periodicity in one direction and form the surface, which is then simulated in periodically repeated slabs. This is an issue in particular for ferroelectric materials with strong electric fields [18,19]. These problems and possible solutions are discussed in some detail in this section.

2.1. Computational details

As in our previous studies on $LiNbO_3$ surfaces [17,20–22], we perform self consistent first-principles calculations in the framework of the density functional theory (DFT) as implemented in the Vienna Ab initio Simulation Package (VASP [23]). All-electron projector-augmented wave potentials [24] within the PW91 formulation of the generalized gradient approximation (GGA) [25] are used. A plane-wave basis set including waves up to an energy of 400 eV is used to expand the electronic wave functions. The atomic positions have been determined minimizing the Hellmann-Feynman forces acting on the single atoms under 0.02 eV/Å. A $4 \times 4 \times 1$ Γ-centered Monkhorst-Pack [26] *k*-point mesh was used to carry out the integration in the Brillouin zone for the simulation of truncated bulk, unreconstructed and $(\sqrt{3} \times \sqrt{3})$ reconstructed surfaces. A $2 \times 2 \times 1$ *k*-point mesh was chosen to sample the much smaller Brillouin zone of the slabs modeling $(\sqrt{7} \times \sqrt{7})$ reconstructed surfaces. The detailed constitution of the slabs used to model surfaces of different periodicity is discussed in the following section. As shown in our previous works, this approach is accurate enough to provide reliable structures and energies for both bulk $LiNbO_3$ in the ferroelectric and paraelectric phase and for $LiNbO_3$ surfaces [17].

2.2. Surface and slab geometries

In most of the works available in the literature, the LN(0 0 0 1) is defined as the positive surface and the LN(000$\bar{1}$) as the negative. However, some authors use the opposite notation. To avoid any confusion, we illustrate here the definition used throughout this work. The [0 0 0 1] crystallographic direction is usually called *z*-direction or *c*-axis. According to the accepted model, the cations in the highly symmetric paraelectric phase are either within (Li^{+1}), or exactly between oxygen layers (Nb^{+5}), as depicted in Fig. 1(a). In the ferroelectric phase, the cations are shifted along the [0 0 0 1] crystallographic direction with respect to the oxygen planes, causing a permanent spontaneous polarization parallel to the cationic displacement. The positive *c*-direction is defined as parallel to the polarization, the negative as antiparallel (see Fig. 1)[1]. Ferroelectric $LiNbO_3$ is thus a stacking of –Nb-O_3-Li– planes along the [0 0 0 1] direction, and is not centrosymmetric. This is an issue within the supercell approach, as the two slab surface terminations cannot be made equivalent and only relative energetic comparisons are possible. In this work we model the LN(0 0 0 1) surface and all its reconstructions with 12 LN trilayers (36 atomic layers) plus surface terminations, resulting in large supercells containing from 60

[1] This defines on turn the positive and the negative *z*-surfaces, created by cutting the crystal perpendicularly to the [0 0 0 1]. Indeed, the standard method of determining the orientation of the *c*-axis is to heat or to compress the crystal in the *c*-direction: by definition the +*c* face becomes negative upon heating or compression. Upon heating or compressing the material, the cations are shifted closer to their paraelectric positions, thereby reducing the net polarization and leaving an excess amount of negative compensating (or depolarization) charge on the +*c* face, which becomes negative [1]. Summarizing, the positive (0 0 0 1) surface is characterized by an electronic charge accumulation, while the negative is characterized by an electronic charge depletion.

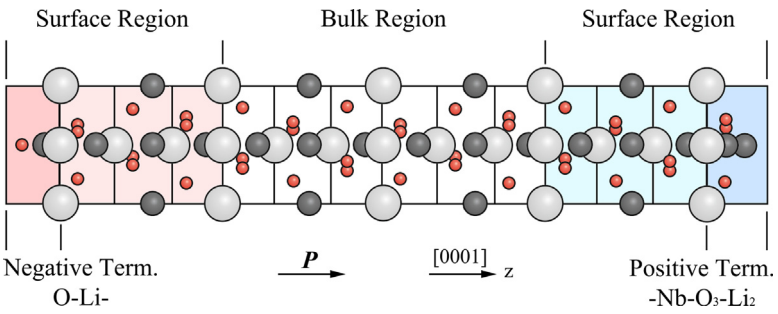

Fig. 2. Slab used to model the thermodynamically stable 1×1 (0 0 0 1) surfaces. The surface termination and the underlying three trilayer (surface region) are free to relax, while the six central trilayer are kept frozen at their bulk positions (bulk region). The positive surface –LN(0 0 0 1)– is at the right hand side, the negative surface –LN(000$\bar{1}$)– at the left hand side. Atomic color coding as in Fig. 1.

atoms (for the simulation of the truncated bulk) up to 460 atoms for the simulation of $(\sqrt{7} \times \sqrt{7})$ reconstructed surfaces. The central part of our slabs (18 atomic layers) are frozen into their ferroelectric positions, while the remaining 18 layers and the surface terminations are free to relax (see Fig. 2). This has two important advantages: on one hand, it saves some computational time, on the other hand, it defines the central part of our slab as a true bulk region, which is not affected by surface effects.[2] This choice is also justified by the results of Levchenko et al. [27], who pointed out that the structural relaxation in the ferroelectric LN(0 0 0 1) surfaces is limited to a few outmost atomic layers. A vacuum region of at least 19 Å separates one slab from its periodic images. As we shall see in the following, cells of this size are thick enough to allow for the definition of macroscopic quantities such as inner – $\boldsymbol{E}_D$– and outer electric field – $\boldsymbol{E}_{EXT}$– from unit cell averages of electrostatic potential $V_H(\mathbf{t})$ and charge densities $\rho(\mathbf{r})$.

2.3. Electrical boundary conditions

Periodic boundary conditions are usually applied both to geometries and to the electrostatic (or Hartree) potential to model bulk systems within the supercell approach. This results in a vanishing macroscopic internal field $\boldsymbol{E}$, even for ferroelectrics with a spontaneous bulk polarization $\boldsymbol{P}_S^{\text{bulk}}$. This situation is illustrated in Fig. 3(a).

A slab wit a net dipole moment perpendicular to the surface will give rise to an electrostatic potential as illustrated in Fig. 3(b). The net dipole moment will in general have contributions from both the bulk polarization and the surface termination. Indeed, a paraelectric material with two non-equivalent surface terminations will give rise to a dipole moment too. This configuration models a surface in the artificial field caused by its neighboring periodic images. Thereby, the electrostatic potential is a continuous function. Neither internal nor external fields have direct physical interpretation as they depend on the cell geometry. Indeed, increasing the thickness of the slab or of the vacuum region the artificial fields become smaller, vanishing in the limit of infinite supercells.

In order to correct for the error introduced by the artificial field in finite slabs, dipole corrections can be applied [28,29]. The correction is introduced by adding an external dipole layer in the vacuum region of the supercell, and leads to the situation depicted in Fig. 3(c), with vanishing external electric field. The electrostatic potential is now discontinuous. However, the discontinuity is localized in the vacuum region, where it is supposed not to affect the calculation.

The polarization $\boldsymbol{P}$ gives rise to surface polarization charges

$$\sigma_S = \boldsymbol{P} \cdot \hat{n}, \tag{1}$$

where $\hat{n}$ is the surface normal.

Meyer and Vanderbilt [19] pointed out that the depolarization field $\boldsymbol{E}_D$ originating from the surface charges might be large enough to destabilize the ferroelectric state: relaxing a polarized slab under periodic boundary conditions corresponding to vanishing external electric field would yield to a paraelectric structure. To overcome this problem they proposed to model polarized slabs with periodic boundary conditions corresponding to vanishing internal field, as illustrated in Fig. 3(d). This boundary condition is equivalent to placing the slabs between the grounded plates of a capacitor, and is

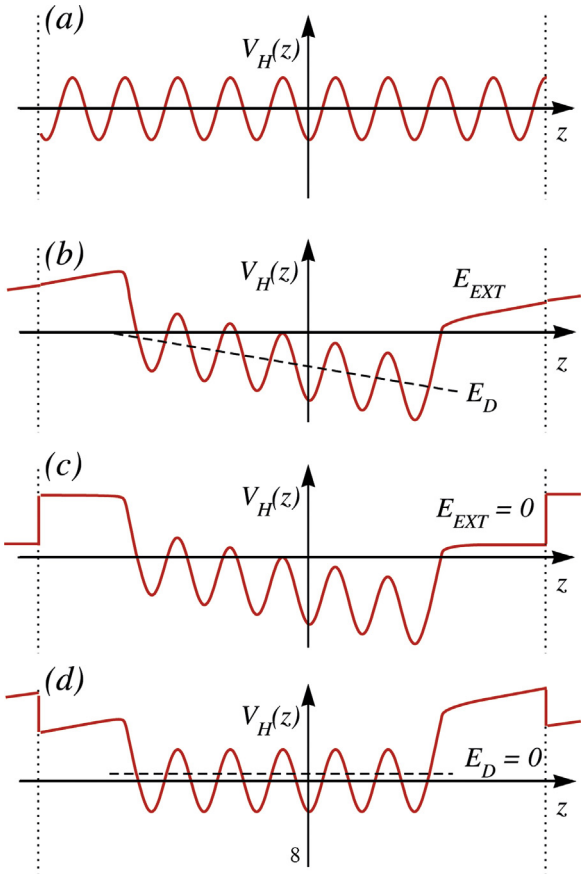

Fig. 3. Planar averaged electrostatic (Hartree) potential of ferroelectric $LiNbO_3$. (a) Bulk supercell, (b) slab of truncated bulk, (c) with vanishing external field, and with vanishing internal electric field (d). Internal (or depolarization) field $\boldsymbol{E}_D$, external field $\boldsymbol{E}_{EXT}$ and slab/supercell boundaries are indicated.

[2] This would not be the correct approach for the simulation of ferroelectric thin films, where ferroelectric and dielectric properties are strongly affected by surface effects. However our focus lies on ferroelectric surfaces and not on ferroelectric thin films.

appropriate to model very thin film geometries, where ferroelectric and dielectric properties are strongly influenced by surface effects [19].

It must be pointed out that none of the described periodic boundary conditions for the electrostatic potential is intrinsically correct and universally applicable. While the vanishing internal field boundaries are the proper conditions far from the surface [19] and thus ideal for the simulation of the "bulk" of thin films, vanishing external field conditions are more appropriate to model the surface itself. Thus, the choice of the appropriate periodic boundary conditions discussed above depends on the system properties one focuses on. Being interested in surface charges, we adopt vanishing external field boundaries. To prevent the slab to relax into the paraelectric state, the central part of our slabs (18 atomic layers) are frozen into their ferroelectric positions, while the remaining 18 layers and the surface terminations are free to relax. This choice is also justified by the results of Levchenko et al. [27], who pointed out that the structural relaxation in the ferroelectric LN(0 0 0 1) surfaces is limited to a few outmost atomic layers. The constitution of the slabs is described in Section 2.2.

The choice of the boundary conditions affects to some extent the calculated the surface charge. The difference in the surface charge calculated with – Fig. 3(c) and without Fig. 3(b) – dipole corrections amount to less than 0.009 C/m^2, which is two orders of magnitude lower than the charges of a LN truncated bulk. For a quantitative estimate of the surface charge, a proper treatment of the pyroelectric effect – currently neglected – will be necessary.

2.4. Macroscopic polarization and polarization charge

As stated by Eq. (1), the polarization charge directly depends on the slab polarization. The polarization component perpendicular to the surface is a well defined quantity, and fully determines the surface charge, provided the polarization is homogeneous. The bulk macroscopic polarization is not a well defined quantity within the supercell approach, though. This is due to the fact as the choice of the supercell is not unique: different supercells characterized by different dipole moments may be chosen to model a given crystal. However, this does not affect the calculation of the surface charge related to a given termination. The macroscopic polarization can be correctly calculated as a Berry phase of the electronic orbitals within the modern theory of polarization [30,31] with respect to a reference phase, usually the corresponding paraelectric phase:

$$\boldsymbol{P} = \int_0^1 \boldsymbol{P}'(\lambda) d\lambda = \boldsymbol{P}(1) - \boldsymbol{P}(0), \tag{2}$$

where $\lambda \in (0, 1)$ is a reaction coordinate which brings the system from the ferroelectric $\boldsymbol{P}(1)$ to the reference (paraelectric) phase $\boldsymbol{P}(0)$. Using the Berry phase approach, we have calculated the spontaneous bulk polarization of stoichiometric LN to be 0.82 C/m^2, in in very good agreement with the commonly accepted value of 0.71 C/m^2 [32], and with the value of 0.86 C/m^2 calculated in a similar manner by Levchenko et al. [27].

In this work, we estimate the surface charge of the positive and negative LN(0 0 0 1) by integrating the planar averaged polarization charge, defined as

$$\rho(z) = \frac{1}{A} \int \int_A \rho(\mathbf{r}) dx dy, \tag{3}$$

from the vacuum center (0) to the cell center (z_{cut}) in both directions. A is the area of the surface unit cell.

$$\sigma_S = \int_0^{z_{\mathrm{cut}}} \rho(z) dz \tag{4}$$

$\rho(\mathbf{r})$ is the charge redistribution due to the surface formation (i.e. the difference with the bulk distribution), so that the slab is charge neutral and the integral over the whole supercell is exactly zero.

Furthermore, for the estimation of the surface charge of an ideal bulk cut, we proceed in the spirit of the Berry approach, and calculate the macroscopic surface charge with respect to a reference phase:

$$\sigma_S^{cut} = \boldsymbol{P} \cdot \hat{\boldsymbol{n}} = (\boldsymbol{P}_F - \boldsymbol{P}_P) \cdot \hat{\boldsymbol{n}} = \sigma_F^{cut} - \sigma_P^{cut} \tag{5}$$

This procedure yields a surface charge which does not depend on the choice of the slab representing the ideal truncated bulk cut, provided the reference phase is chosen carefully. In our case, the reference structure is a corresponding slab of LN in the paraelectric phase. We remark that the method is only applied in Section 3.1 for the calculation of an ideal LN bulk cut. For any given termination, the polarization component perpendicular to the surface is well defined, and fully determines the surface charge.

The proper choice of the integration limits of Eq. (4) is a delicate task: the charge density oscillations within the slab are larger than the electronic charge accumulation/depletion we want to estimate, and the value of σ_S is extremely dependent on the choice of z_{cut}. We circumvent the choice of some geometrical point z_{cut} to perform "the cut" by dividing the slab into atomic layers. In an small slab consisting of two Nb-O_3-Li tri-layers stapled along the z-direction, the lower trilayer builds the lower (negative) surface, while the upper trilayer builds the upper (positive) surface. Then, the charges of the upper (or lower) slab are summed up to calculate the surface charge. To assign a volume – and the corresponding included charge – to an atomic layer, we use the definition of Bader atomic volumes and Bader charges [33]. This process turns out to be very robust and less influenced by computational parameters. Convergence tests have shown that the calculated surface charge converges quickly with respect to number of grid-points in real space. Performing the calculation with or without the core electrons charge does not modify the results within the numerical accuracy.

Summarizing, the calculation of the surface charges is a three step process. (1) At first the total electronic charge of the slab representing a given termination is calculated self-consistently and then partitioned by Bader volumes into upper and lower slab half. (2) In a second step, the charge redistribution $\rho(\mathbf{r})$ of Eq. (4) is obtained by subtracting the Bader charges of the corresponding atoms in the bulk phase. (3) Finally, the charge redistribution of the Bader volumes within the upper and within the lower slab half are added up: the resulting sum is the surface charge σ_S.

The method applied to calculate the surface charge does not represent a criterion to actually predict stable surface reconstructions, which are determined by the *ab inito* thermodynamics alone. It rather allows a quick estimation of the surface charge of all the terminations.

3. Results

3.1. Truncated bulk

The validity of the approach described in the previous section is demonstrated with the following example, in which we calculate the surface charge of a truncated bulk of LN. Thereby the atomic positions are kept fixed in their bulk positions, only the electronic distribution is calculated self-consistently. Unrelaxed ferroelectrics are not affected by the artificial errors arising relaxing surface atoms with improper periodic boundary conditions and are therefore ideal testbeds to validate our method. Thereby, the bulk polarization of the material represents an upper bound of the calculated surface charge. Indeed, surface charges in a calculation can be

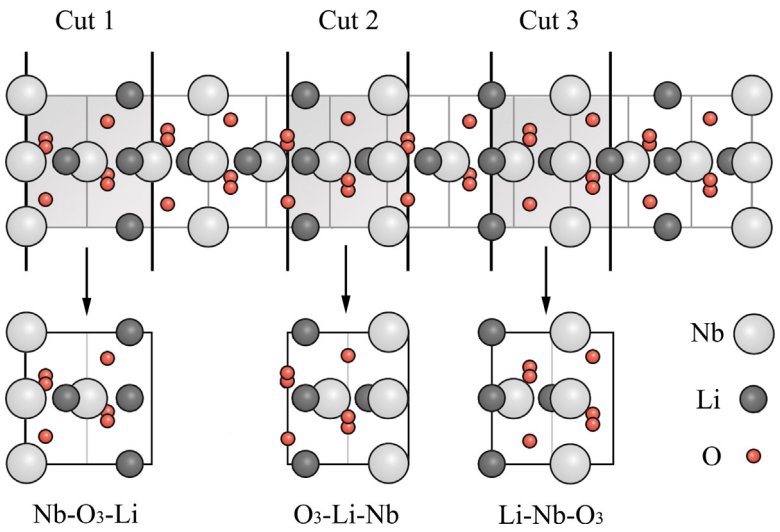

Fig. 4. Ferroelectric bulk $LiNbO_3$ can be cut perpendicularly to the [0 0 0 1] direction at three non-equivalent planes, resulting in a Li, O_3, and Nb termination (Cut 1, Cut 2 and Cut 3 in the picture). Different cuts are modeled by slabs with different electric dipole moment, both in size and direction. Only slabs containing an integer number of LN formula units are considered.

partially compensated by the electron transfer through the band gap. Therefore, calculated surface charges even for an unrelaxed slab of an excellent isolator such as $LiNbO_3$ might be lower than the charges calculated from bulk polarization.

Considering ferroelectric LN as a stacking of -Nb-O_3-Li- atomic layers along the [0 0 0 1] crystallographic direction, three non equivalent atomic cuts can be discriminated. Cutting the crystal above a Li-layer (cut 1 in Fig. 4), the slab representing the crystal will be a succession of Nb-O_3-Li-trilayers. Cutting the crystal above a Nb-layer, the slab will be a succession of O_3-Li-Nb-trilayers (cut 2 in Fig. 4). Finally, cutting the crystal above an oxygen layer, the slab will be a succession of Li-Nb-O_3-trilayers (cut 3 in Fig. 4). 12-Trilayers are used for the calculations. For the sake of simplicity, we only consider slabs containing an integer number of LN formula units, however our discussion can be extended to supercells of non-stoichiometric composition.

The slabs built to model these cuts are characterized by very different electric dipole moments, both in magnitude and direction, resulting in three different surface charge values σ_F^{cut}. The surface charge of the different cuts has been calculated as described by Eq. (4), and the result are reported in Table 1. However, the total surface charge σ_S^{cut} has to be calculated with respect to a reference phase, as described by Eq. (5). Thereby, just as in case of the calculation of the volume spontaneous polarization via Berry phase, the correct choice of the (paraelectric) reference phase is crucial. In the case of a LN truncated bulk, it is relatively easy to find the cuts of the paraelectric phase corresponding to those of the ferroelectric phase. These are illustrated in Fig. 5 and called cut 1′, cut 2′ and cut 3′ for the sake of simplicity. Calculating the corresponding surface charge σ_P^{cut} and inserting it in Eq. (5), one obtains roughly the same value of the surface charge for all the three cuts, namely 0.65 ± 0.01 $e/(1 \times 1)$-surface unit cell, as reported in Table 1.

Table 1
Surface charge calculated at the positive LN(0 0 0 1) for a ferroelectric slab (σ_F^{cut}), for the corresponding reference (paraelectric) phase (σ_P^{cut}) and the value σ_S^{cut} calculated with Eqs. (4) and (5). The definition of the surface cuts is in Fig. 4. All values in $e/(1 \times 1)$-surface unit cell.

	Cut 1	Cut 2	Cut 3
σ_F^{cut}	−0.66	1.95	−1.64
σ_P^{cut}	−1.31	1.31	−2.30
σ_S^{cut}	0.65	0.64	0.66

Table 2
Surface charge calculated at the positive LN(0 0 0 1) for a Cut 1 termination with slabs containing a different number of atomic layers. σ_F^{cut}, σ_P^{cut} and σ_S^{cut} have the same meaning as in Table 1. All values in $e/(1 \times 1)$-surface unit cell.

Layer number	18	24	30	36
σ_F^{cut}	−0.62	−0.64	−0.65	−0.66
σ_P^{cut}	−1.28	−1.30	−1.31	−1.31
σ_S^{cut}	0.66	0.66	0.66	0.65

As a second step, the value of σ_S^{cut} has been calculated with slabs containing a different number n of atomic layers. The dependence of σ_S^{cut} on the number of atomic layers is only marginal, as reported in Table 2. However, the value of σ_S^{cut} for cells of infinite size can be extrapolated plotting its dependence on $1/n$, as reported in Fig. 6. The extrapolated value of the surface charge σ_S^{cut} = 0.64 e / (1×1)-surface unit cell, corresponding to 0.46 C/m^2 is somewhat lower, yet in reasonable agreement with the value expected from the bulk polarization. The deviation from the expected value might be traced back to the uncertainties introduced by the supercell approach discussed in Section 2.3, to a partial compensation by the electron transfer through the band gap in the calculation, and by the choice of partitioning the cell by Bader volumes. Thus, the calculated value does not allow for a quantitative prediction of the surface charge, however it will suffice for a qualitative discussion.

As a third step we calculated the surface charge for slabs of different periodicity. The calculated values are reported in Table 3. As expected, the charge σ_S^{cut} does not depend on the area of the unit cell used for the calculation.

Our method represents an important step towards the reconciliation of macroscopic and microscopic picture. The surface charge calculated with the three microscopic models is the same, and represents the polarization charge of an ideal bulk cut in our calculation.

Table 3
Surface charge calculated at the positive LN(0 0 0 1) for a Cut 1 termination with slabs of different periodicity. σ_F^{cut}, σ_P^{cut} and σ_S^{cut} have the same meaning as in Table 1. All values in $e/(1 \times 1)$-surface unit cell.

Periodicity	1×1	$\sqrt{3} \times \sqrt{3}$	$\sqrt{7} \times \sqrt{7}$
σ_F^{cut}	−0.62	−0.65	−0.62
σ_P^{cut}	−1.28	−1.31	−1.28
σ_S^{cut}	0.66	0.66	0.66

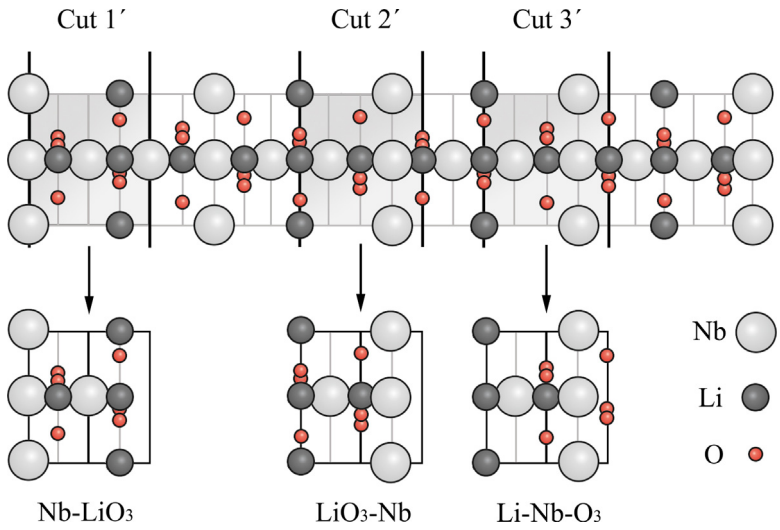

Fig. 5. Paraelectric bulk $LiNbO_3$ can be cut perpendicularly to the [0 0 0 1] direction at two non-equivalent planes, resulting in a LiO_3 and Nb termination (Cut 1′ and Cut 2′ in the picture). Cut 1′ and Cut 2′ represent the paraelectric reference phase to Cut 1 and Cut 2 of the ferroelectric phase in Fig. 4, Cut 3′ corresponds to the ferroelectric Cut 3.

3.2. Phase diagram

After validating the method applying it to an ideal truncated bulk, we proceed with the calculation of the surface charge of realistic surfaces, which are characterized by relaxation and reconstructions. Levchenko et al. [27] predicted the phase diagram of the LN(0 0 0 1) from *ab initio* thermodynamics, finding the stable terminations at the two surfaces to be rather temperature independent. In this work, however, only surfaces with 1×1 periodicity had been considered. Later, AFM measurements and DFT models including cells of different periodicity showed that different reconstructions might be formed at different temperature regimes [17]. Some of them might be inhibited by the presence of adsorbates and can only occur in vacuum. The corresponding phase diagram (now including reconstructed surfaces) has been calculated as a function of the chemical potentials of lithium and oxygen. As the goal of this investigation is to search for a correlation between surface charge and temperature, we first convert the phase diagram of the LN(0 0 0 1) of Ref. [17] in a function of temperature and Li partial pressure. This can be done within the ideal gas approximation [34], as explained in our previous works [22].

The result of this transformation is shown in Fig. 7 for the positive as well as for the negative face of the LN(0 0 0 1). At low temperatures, at the positive face a $(\sqrt{3} \times \sqrt{3})$ reconstruction built adding 2 Li atoms to the stable termination is formed. With growing temperature, reconstructions containing less Li are formed, till after 1000 K the (1×1) stable reconstruction predicted by Levchenko et al. [27] is restored. At the negative surface, a $(\sqrt{7} \times \sqrt{7})$ reconstruction built adding 2 Li and 2 O atoms to the stable termination is formed at lower temperatures. With increasing temperatures, a further a $(\sqrt{7} \times \sqrt{7})$ reconstruction built adding 2 Li and a single O atoms and a $(\sqrt{3} \times \sqrt{3})$ reconstruction formed adding a single oxygen atom to the stable termination are formed.

The succession of the surface reconstructions at different temperatures is shown in Table 4. The nominal charge added by the reconstruction at the positive side – also listed in the table – is

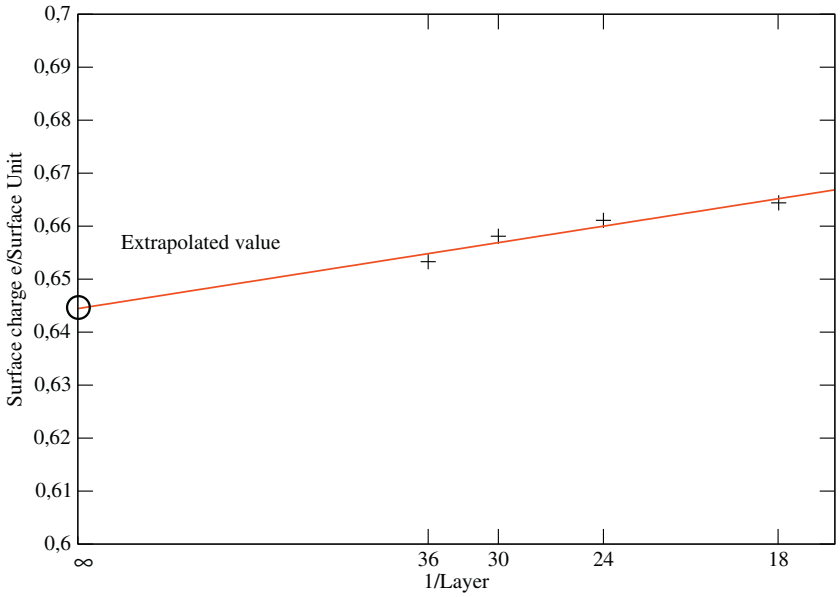

Fig. 6. Surface-charge density σ_S^{cut} as a function of the number n of atomic layer in the slab. The solid line is the linear interpolation of the calculated points, the extrapolated value for ideal infinite slabs is indicated.

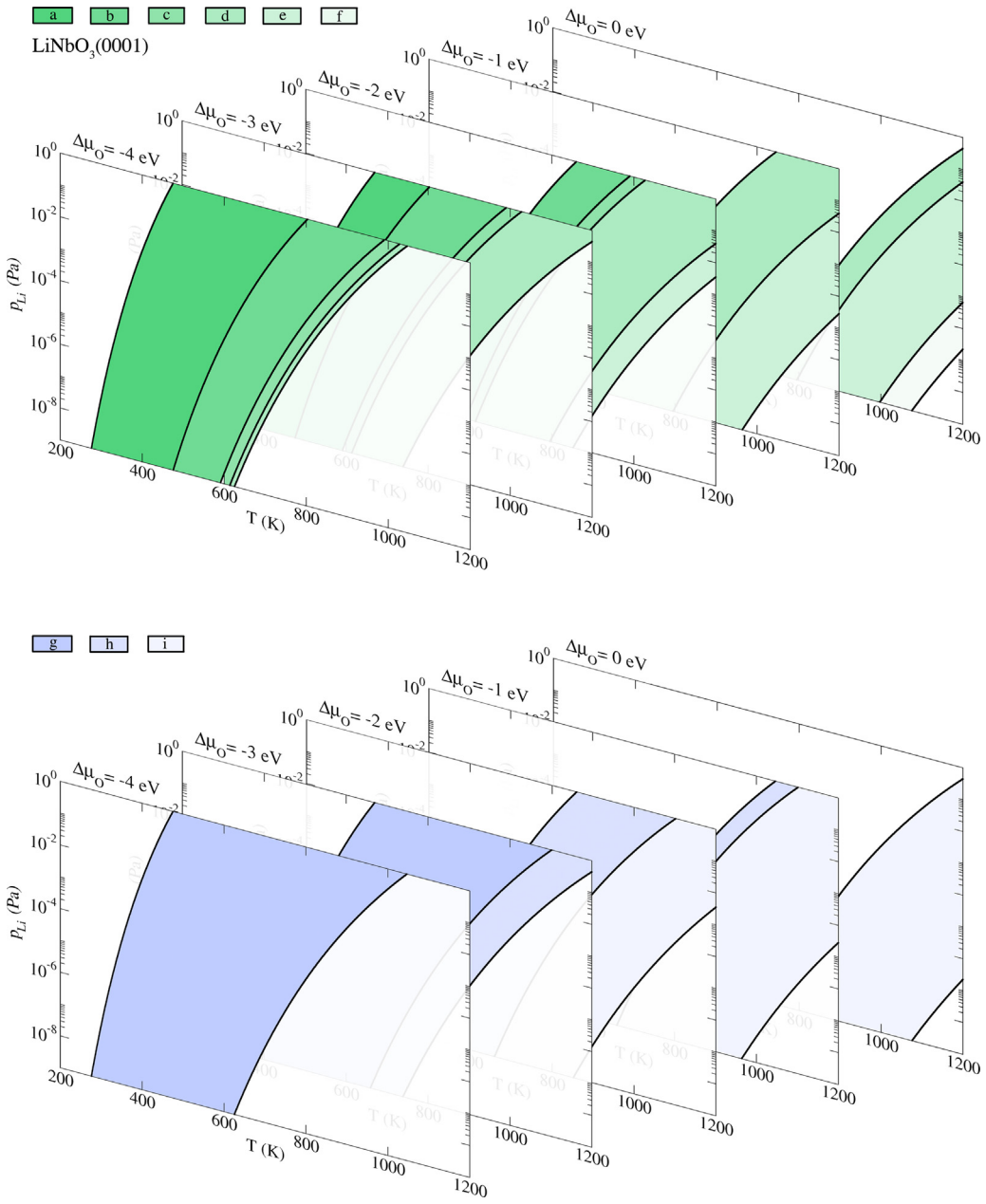

Fig. 7. Calculated phase diagram of the positive (upper part) and negative (lower part) LN(0 0 0 1) surface as a function of temperature and pressure. The terminations (a), . . ., (f) are explained in Table 4.

Table 4
Surface charge calculated at the positive LN(0 0 0 1) for surface terminations of different periodicity. The temperature range is assigned assuming a Li partial pressure of 10^{-8} Pa. Note that not all the surface reconstructions are allowed for arbitrary values of μ_O, as shown in Fig. 7. All charges are expressed in $e/(1 \times 1)$-surface unit cell. Positive therminations in the upper part, negative terminations in the lower part.

Period.	Term.	Stab. range	Nom. charge	σ_S
$(\sqrt{3} \times \sqrt{3})$	+2Li (a)	250–450 K	0.66	+0.077
$(\sqrt{7} \times \sqrt{7})$	+3Li (b)	450–600 K	0.43	−0.019
$(\sqrt{3} \times \sqrt{3})$	+Li (c)	600–620 K	0.33	−0.052
$(\sqrt{7} \times \sqrt{7})$	+2Li (d)	620–820 K	0.29	−0.041
$(\sqrt{7} \times \sqrt{7})$	+Li (e)	820–1050 K	0.14	−0.099
(1×1)	– (f)	1050–1150 K	0.00	−0.104
$(\sqrt{3} \times \sqrt{3})$	+O (i)	680–1150 K	0.66	+0.004
$(\sqrt{7} \times \sqrt{7})$	+Li+O (h)	620–680 K	0.14	−0.071
$(\sqrt{7} \times \sqrt{7})$	+2Li+O (g)	250–620 K	0.00	−0.087

a decreasing function of the temperature. However, the effective surface charge σ_S has not necessarily to be directly proportional to the nominal charge brought by the adsorbed species. Therefore, we calculate σ_S with the method previously illustrated.

3.3. Relaxed surface

At first, we calculate the relaxed surface with (1×1) periodicity. Differently from the ideal truncated bulk termination, where the expected polarization charge is in principle known, there is no reference value for the clean, relaxed LN(0 0 0 1) surfaces in vacuum, so that our calculations have predictive character. The only work we are aware of, in which the surface charge of the LN(0 0 0 1) has been measured [35], has been performed in air. The measured charge refers therefore to a surface on which a lot of adsorbates (both neutral molecules and radicals) have contributed to stabilize the surface by charge compensation. This is of course rather different

from the ideal, clean and adsorbate free surfaces we model. Indeed, a much smaller surface charge of 140 $\mu C/m^2$ is measured for congruently melt, nominally undoped $LiNbO_3$ crystals, i.e. a factor of 2×10^{-4} smaller than the spontaneous polarization of 0.71 C/m^2.

The calculated surface charge of a $LiNbO_3$ slab terminated according to the stable surface structure (see Fig. 2) amounts to 0.104 $e/(1 \times 1)$-surface unit cell corresponding to about 16% of the surface charge of the ideal ferroelectric bulk cut. This is in agreement with the predictions of Levchenko and Rappe [27]. In their work, they have proposed a ionic model based on formal oxidation states to explain the stability of the preferred terminations of positive and negative surfaces by passivation of surface charges with ions. According to this model, the surface charge of a truncated bulk LN(0 0 0 1) surface is reduced by 80% by the formation of the stable terminations, a value very close to the reduction by about 84% calculated in this work. The experiment of Ref. [35]shows that the surface charge must be compensated almost completely, because maintaining a non-zero surface charge is energetically unfavorable. The non-complete charge compensation resulting from the calculations is a result of limitations in the models, such as limited unit cell sizes, and most of all limited number of adsorbate types.

3.4. Reconstructed surface

Some of the reconstructions we are investigating are formed at high temperatures. At these temperature the LN crystal is much closer to the paraelectric phase than at room temperature due to the pyroelectric nature of the material. The spontaneous polarization and therefore the surface charge are thus strongly reduced. Pyroelectricity is not included in our model, therefore the calculated σ_S is not quantitatively correct value. Nonetheless our calculations can be used to compare the relative surface charge of different terminations.

The calculated values of the surface charge σ_S for reconstructions formed at different temperatures are complied in Table 4. The σ_S values for reconstruction at the positive face are calculated with the stable (1×1) termination at the negative side and vice versa. It is thus possible to estimate the efficiency of the single reconstructions in charge compensation. In all the investigated cases, the formation of an adatom-induced reconstruction yields to a polarization charge reduction with respect to the stable (1×1) termination, thus stabilizing the suface. It can be observed that the lowering of the surface charge is roughly proportional to the nominal charge of the adsorbed adatoms. The $(\sqrt{3} \times \sqrt{3})$ reconstruction formed by the additon of two Li-atoms at the positive side and the $(\sqrt{3} \times \sqrt{3})$ reconstruction formed by the additon of one O-atom at the negative side (nominal additional charge of ± 0.66 electrons per (1×1)-surface unit cell) lead to an overcompensation of the surface charge.

We find that with increasing temperature surface terminations which reduce the polarization charge to a lesser extent are favored. However, this does not mean that with increasing temperature a larger surface charge will be measured. Indeed, the surface charge in real samples will be a decreasing function of the temperature, as with increasing temperature the cations move closer to their paraelectric configuration, thereby reducing the net polarization. Thus, reconstructions with a minor impact on the surface charge will be able to stabilize it. At temperatures over 1200 K, the spontaneous polarization will be low enough that no surface reconstruction is needed and the 1×1 periodicity is recovered. The lowered surface charge of all the stable reconstructed surfaces suggests that the surface charge compensation is a major driving force for the observed morphologic transformations. We want to remark that the stability of the high temperature reconstruction is governed exclusively by the surface thermodynamics.

4. Conclusions

A method for the calculation of the macroscopic surface charge within the periodically repeated slab approach has been proposed and applied to ferroelectric LN surfaces. The surface charge of an ideal truncated bulk has been found to be σ_S^{cut}=0.46 C/m^2. This surface charge is reduced by about 84% upon formation the stable (1×1) surface structure found in Ref. [27,20]. The surface reconstructions recently revealed by AFM techniques [17] further reduce the polarization charge, thus stabilizing the surface. Indeed, all the thermodynamically stable surface reconstruction lead to a lowering of the polarization charge, showing that the surface charge compensation is the major driving force for the observed morphologic transformations. We want to remark that our models represent ideal surfaces of stoichiometric $LiNbO_3$ in an environment free of foreign adsorbates. In congruent material the outgasing of LiO already at moderate temperatures (≈600 K) is severely deteriorating crystalline quality and affecting the surface composition. This is not the case for stoichiometric material [36]. In addition, in real surfaces the presence of external adsorbates, surface defects and step edges will further reduce the surface charge.

References

[1] R.S. Weis, T.K. Gaylord, Lithium-niobate – summary of physical-properties and crystal-structure, Applied Physics A: Materials Science and Processing 37 (4) (1985) 191–203.

[2] T.-C. Lee, J.-T. Lee, M.A. Robert, S. Wang, T.A. Rabson, Surface acoustic wave applications of lithium niobate thin films, Applied Physics Letter 82 (2) (2003) 191–193, http://dx.doi.org/10.1063/1.1534413, URL http://scitation.aip.org/content/aip/journal/apl/82/2/10.1063/1.1534413

[3] G. Namkoong, K.-K. Lee, S.M. Madison, W. Henderson, S.E. Ralph, W.A. Doolittle, III-Nitride integration on ferroelectric materials of lithium niobate by molecular beam epitaxy, Applied Physics Letter 87 (17) (2005) 171107, http://dx.doi.org/10.1063/1.2084340, URL http://scitation.aip.org/content/aip/journal/apl/87/17/10.1063/1.2084340

[4] D. Li, M.H. Zhao, J. Garra, A.M. Kolpak, A.M. Rappe, D.A. Bonnell, J.M. Vohs, Direct in situ determination of the polarization dependence of physisorption on ferroelectric surfaces, Nature Materials 7 (6) (2008) 473–477, http://dx.doi.org/10.1038/nmat2198.

[5] M. Stock, S. Dunn, $LiNbO_3$ – a new material for artificial photosynthesis, IEEE Transactions on Ultrasonics, Ferroelectrics, and Frequency Control 58 (9) (2011) 1988.

[6] M. Stock, S. Dunn, Influence of the ferroelectric nature of lithium niobate to drive photocatalytic dye decolorization under artificial solar light, Journal of Physical Chemistry C 116 (39) (2012) 20854–20859.

[7] R. Ferris, B. Yellen, S. Zauscher, Ferroelectric thin films in fluidic environments: a new interface for sensing and manipulation of matter, Small 8 (1) (2011) 28–35.

[8] S. Huang, J. Luo, H.-L. Yip, A. Ayazi, X.-H. Zhou, M. Gould, A. Chen, T. Baehr-Jones, M. Hochberg, A.K.Y. Jen, Efficient poling of electro-optic polymers in thin films and silicon slot waveguides by detachable pyroelectric crystals, Advanced Materials 24 (10) (2011) OP42–OP47.

[9] F. Merola, S. Grilli, S. Coppola, V. Vespini, S. De Nicola, P. Maddalena, C. Carfagna, P. Ferraro, Reversible fragmentation and self-assembling of nematic liquid crystal droplets on functionalized pyroelectric substrates, Advanced Functional Materials 22 (15) (2012) 3267–3272.

[10] Y. Yun, M. Li, D. Liao, L. Kampschulte, E. Altman, Geometric and electronic structure of positively and negatively poled $LiNbo_3$(0 0 0 1) surfaces, Surface Science 601 (19) (2007) 4636–4647, http://dx.doi.org/10.1016/j.susc.2007.08.001, URL http://www.sciencedirect.com/science/article/pii/S0039602807008254

[11] A. Saito, H. Matsumoto, S. Ohnisi, M. Akai-Kasaya, Y. Kuwahara, M. Aono, Structure of atomically smoothed $LiNbO_3$(0 0 0 1) surface, Japanese Journal of Applied Physics 43 (4B) (2004) 2057–2060.

[12] K. Tabata, T. Choso, A. Murakami, E. Suzuki, Topmost surface analysis of a z-cut $LiNbO_3$, by coaxial impact-collision ion scattering spectroscopy, Surface Science 402 (1–3) (1998) 487–490.

[13] J.M.P. Martirez, E.H. Morales, W.A. Saidi, D.A. Bonnell, A.M. Rappe, Atomic and electronic structure of the $BaTiO_3$(0 0 1) $(\sqrt{5} \times \sqrt{5})r26.6^\circ$ surface reconstruction, Physics Review Letter 109 (2012) 256802, http://dx.doi.org/10.1103/PhysRevLett.109.256802.

[14] M.R. Castell, Scanning tunneling microscopy of reconstructions on the $SrTiO_3$(0 0 1) surface, Surface Science 505 (2002) 1–13, http://dx.doi.org/10.1016/S0039-6028(02)01393-6, URL http://www.sciencedirect.com/science/article/pii/S0039602802013936

[15] G.-z. Zhu, G. Radtke, G.A. Botton, Bonding and structure of a reconstructed (0 0 1) surface of $SrTiO_3$ from TEM, Nature 490 (7420) (2012) 384–387.

[16] S. Rode, R. Hölscher, S. Sanna, S. Klassen, K. Kobayashi, H. Yamada, W.G. Schmidt, A. Kühnle, Atomic-resolution imaging of the polar $(000\bar{1})$ surface of $LiNbO_3$ in aqueous solution by frequency modulation atomic force microscopy, Physics Review B 86 (2012) 075468, http://dx.doi.org/10.1103/PhysRevB.86.075468.
[17] S. Sanna, S. Rode, R. Hölscher, S. Klassen, C. Marutschke, K. Kobayashi, H. Yamada, W.G. Schmidt, A. Kühnle, Charge compensation by long-period reconstruction in strongly polar lithium niobate surfaces, Physics Review B 88 (2013) 115422, http://dx.doi.org/10.1103/PhysRevB.88.115422.
[18] L. Fu, E. Yashenko, L. Resca, R. Resta, Hartree-Fock studies of surface properties of $BaTiO_3$, Physical Review B 60 (1999) 2697.
[19] B. Meyer, D. Vanderbilt, Ab initio study of $BaTiO_3$ and $PbTiO_3$ surfaces in external electric fields, Physical Review B 63 (20) (2001) 205426.
[20] S. Sanna, W.G. Schmidt, Lithium niobate *x*-cut, *y*-cut, and *z*-cut surfaces from ab initio theory, Physics Review B 81 (2010) 214116, http://dx.doi.org/10.1103/PhysRevB.81.214116.
[21] S. Sanna, A.V. Gavrilenko, W.G. Schmidt, Ab initio investigation of the $LiNbO_3(0001)$ surface, Physica Status Solidi C 7 (2) (2010) 145–148, http://dx.doi.org/10.1002/pssc.200982456.
[22] S. Sanna, R. Hölscher, W.G. Schmidt, Polarization-dependent water adsorption on the $LiNbO_3(0001)$ surface, Physics Review B 86 (2012) 205407, http://dx.doi.org/10.1103/PhysRevB.86.205407.
[23] G. Kresse, J. Furthmüller, Efficient iterative schemes for ab initio total-energy calculations using a plane-wave basis set, Physics Review B 54 (16) (1996) 11169–11186, http://dx.doi.org/10.1103/PhysRevB.54.11169.
[24] P.E. Blöchl, Projector augmented-wave method, Physics Review B 50 (24) (1994) 17953–17979.
[25] J.P. Perdew, W. Yue, Accurate and simple density functional for the electronic exchange energy: generalized gradient approximation, Physics Review B 33 (12) (1986) 8800–8802, http://dx.doi.org/10.1103/PhysRevB.33.8800.
[26] H.J. Monkhorst, J.D. Pack, Special points for brillouin-zone integrations, Physics Review B 13 (1976) 5188–5192, http://dx.doi.org/10.1103/PhysRevB.13.5188.
[27] S.V. Levchenko, A.M. Rappe, Influence of ferroelectric polarization on the equilibrium stoichiometry of lithium niobate (0001) surfaces, Physics Review Letter 100 (2008) 256101, http://dx.doi.org/10.1103/PhysRevLett.100.256101.
[28] L. Bengtsson, Dipole correction for surface supercell calculations, Physics Review B 59 (1999) 12301–12304, http://dx.doi.org/10.1103/PhysRevB.59.12301.
[29] J. Neugebauer, M. Scheffler, Adsorbate-substrate and adsorbate-adsorbate interactions of na and k adlayers on Al(111), Physics Review B 46 (1992) 16067–16080, http://dx.doi.org/10.1103/PhysRevB.46.16067.
[30] D. Vanderbilt, R.D. King-Smith, Electric polarization as a bulk quantity and its relation to surface charge, Physics Review B 48 (1993) 4442–4455, http://dx.doi.org/10.1103/PhysRevB.48.4442.
[31] R. Resta, Modern theory of polarization in ferroelectrics, Ferroelectrics 151 (1) (1994) 49–58.
[32] F. Johann, E. Soergel, Quantitative measurement of the surface charge density, Applied Physics Letters 95 (23) (2009), http://dx.doi.org/10.1063/1.3269606, URL http://www.scitation.aip.org/content/aip/journal/apl/95/23/10.1063/1.3269606
[33] R.F.W. Bader, Atoms in Molecules – A Quantum Theory, Oxford University Press, New York, 1990.
[34] L.D. Landau, E.M. Lifshitz, Statistical Physics, Part I, 3rd ed., Butterworth-Heinemann, Oxford, 1981.
[35] F. Johann, E. Soergel, Quantitative measurement of the surface charge density, Applied Physics Letter 95 (2009) 232906–232908, http://dx.doi.org/10.1063/1.3269606.
[36] A. Lushkin, V. Nazarenko, K. Pilipchak, V. Shnyukov, A. Naumovets, The impact of annealing and evaporation of $LiNbO_3$ crystals on their surface composition, Journal of Physics D – Applied Physics 32 (1) (1999) 9–15.